

Cationic-competition-induced monoclinic phase in high piezoelectric $(\text{PbSc}_{1/2}\text{Nb}_{1/2}\text{O}_3)_{1-x}-(\text{PbTiO}_3)_x$ compounds

R. Haumont,¹ B. Dkhil,¹ J. M. Kiat,^{1,2} A. Al-Barakaty,³ H. Dammak,¹ and L. Bellaïche³

¹*Laboratoire Structures, Propriétés et Modélisation des Solides, Ecole Centrale Paris, CNRS-UMR8580, Grande Voie des Vignes 92295, Châtenay-Malabry Cedex, France*

²*Laboratoire Léon Brillouin, CE Saclay, CNRS-UMR12, 91191 Gif-sur-Yvette Cedex, France*

³*Department of Physics, University of Arkansas, Fayetteville, Arkansas 72701, USA*

(Received 16 December 2002; revised manuscript received 6 March 2003; published 30 July 2003)

A global picture for the structural evolution in the relaxor-ferroelectric solid solution $(\text{PbSc}_{1/2}\text{Nb}_{1/2}\text{O}_3)_{1-x}-(\text{PbTiO}_3)_x$ is proposed. Thanks to x-ray profile analysis and Rietveld neutron powder refinement, a monoclinic phase has been evidenced in the morphotropic region (i.e., $x \approx 0.43$). This lower-symmetry phase “bridges” the rhombohedral Ti-poor phase ($x \leq 0.26$) with the tetragonal Ti-rich phase ($x \geq 0.55$), in a similar way as in $\text{PbMg}_{1/3}\text{Nb}_{2/3}\text{O}_3$ - PbTiO_3 or $\text{Pb}(\text{Zn}_{1/3}\text{Nb}_{2/3})\text{O}_3$ - PbTiO_3 . For weak titanium concentration, we observe a macroscopic rhombohedral state with local monoclinic symmetry resulting from the combination between Pb and Sc/Nb/Ti shifts along [001] and [111] directions, respectively. Cationic competition with Ti doping increases the coherence length of this short-range monoclinic phase, which becomes long range in the morphotropic region. This intermediate monoclinic phase is in complete agreement with our first-principles calculations which predict Pm or Cm space groups. It has been shown that these ones are very close to each other in the free-energy space, and a minor change of atomic distribution and/or a slight modification in composition or in stoichiometry is enough to alter the space group of the monoclinic ground state. Finally, in the Ti-rich region, the monoclinic ground state is destroyed in favor of a tetragonal phase.

DOI: 10.1103/PhysRevB.68.014114

PACS number(s): 61.50.-f

I. INTRODUCTION

One of the most interesting and studied groups of disordered compounds undergoing structural phase transitions are the so-called relaxors.¹ The main structural feature of relaxors is the random occupation of equivalent positions by different heterovalent ions. This chemical disorder results in the destruction of the normal ferroelectric phase transition and the appearance of physical properties similar to those of disordered magnets. The associated dielectric susceptibility exhibits an unusual response, strongly dependent on frequency and with very high values over a broad range of temperatures.² The relaxor state is then characterized by the frustration of local polarizations which can prevent long-range ferroelectric order from developing completely. Most of the relaxors are lead oxides belonging to the class of perovskites with either the general formula $\text{Pb}(B')_{1/3}(B'')_{2/3}\text{O}_3$ ($B' = \text{Mg}^{2+}, \text{Zn}^{2+}, \dots; B'' = \text{Nb}^{5+}, \text{Ta}^{5+}, \dots$), i.e., 1:2-type compounds or $\text{Pb}(B')_{1/2}(B'')_{1/2}\text{O}_3$ ($B' = \text{Sc}^{3+}, \text{In}^{3+}, \dots; B'' = \text{Nb}^{5+}, \text{Ta}^{5+}, \dots$), i.e., 1:1-type compounds.

In the case of 1:2-type compounds such as $\text{PbMg}_{1/3}\text{Nb}_{2/3}\text{O}_3$ (PMN), considered by most researchers to be the prototype of relaxors, the disorder results from the random occupation of the B site of the perovskite by two cations of different valences, namely, Mg^{2+} and Nb^{5+} . Charge neutrality imposes the Mg:Nb stoichiometry of 1:2, while the mixed-valence character of the B site produces random electric-field gradients and a locally broken translational symmetry.³ Below a certain temperature, polar nanometric regions take place and freeze out.^{4,5} No phase transition into a macroscopic ferroelectric phase occurs, the average structure remaining cubic down to 5 K.^{6,7} But an

induced ferroelectric phase can be realized by means of partial substitution,^{8,9} external electric field,^{10–12} or pressure.¹³ Therefore existence or absence of phase transition is not a necessary condition for the relaxation phenomenon. Indeed, both 1:2- and 1:1-type ferroelectric relaxors such as $\text{Pb}(\text{Zn}_{1/3}\text{Nb}_{2/3})\text{O}_3$ (PZN) (Ref. 14) and $\text{Pb}(\text{Sc}_{1/2}\text{Nb}_{1/2})\text{O}_3$ (PSN),^{15,16} respectively, undergo a spontaneous phase transition from a cubic to a rhombohedral phase.

PSN is of a special interest because the degree of ordering of Sc^{3+} - and Nb^{5+} -type ions can be controlled by thermal treatment, due to a high-temperature order-disorder transformation, which influences the dielectric behavior.^{15–17} This feature provides promising directions for future experimental and theoretical research; indeed it has been shown from a first-principles-derived approach^{18–21} that some specific arrangements between Sc^{3+} and Nb^{5+} (i) greatly enhance the electromechanical responses, (ii) lead to currently unobserved ground states of orthorhombic and monoclinic symmetries (while the disordered material adopts a well-known rhombohedral ground state), and (iii) can considerably shift the Curie temperature. In this heterovalent system, electrostatic interactions among Sc^{3+} and Nb^{5+} ions are then found to be very important. In addition, the stabilized structure is also conditioned by Pb^{2+} ions forming short Pb-O bonds.¹⁸

Recently, relaxor-based single crystals such as $(\text{PbMg}_{1/3}\text{Nb}_{2/3}\text{O}_3)_{1-x}-(\text{PbTiO}_3)_x$ (PMN-PT) and $(\text{PbZn}_{1/3}\text{Nb}_{2/3}\text{O}_3)_{1-x}-(\text{PbTiO}_3)_x$ (PZN-PT) have been reported to exhibit excellent piezoelectric properties, much better than the well-known $\text{PbZr}_x\text{Ti}_{1-x}\text{O}_3$ (PZT) polycrystalline ceramics,²² and have attracted attention for their potential in various applications.^{23–25} Though clearly promising for transducers and actuators, their relatively low Curie tem-

perature of around 440 K (for $x=35\%$ and $x=9\%$, respectively, in PMN-PT and PZN-PT) may greatly limit their usefulness in many fields such as automotive and aerospace sensors where a broad temperature range is required. Thus new relaxor-PT systems with both high transition temperatures and large piezoelectric coefficients are desired.

For this purpose the $(\text{PbSc}_{1/2}\text{Nb}_{1/2}\text{O}_3)_{1-x}(\text{PbTiO}_3)_x$ (PSN-PT) system can be an attractive candidate. Indeed Tenenry, Hang, and Novak²⁶ and Yamashita²⁷ reported in this system very high permittivity and an electromechanical coupling factor k_p which should make it the best relaxor-PT ceramic material for large- k applications. However, up to now this system has attracted less attention than other lead-based compounds.

The high electromechanical performance characteristics of the relaxor-PT solid solutions are found for compositions at or near the morphotropic phase boundary (MPB) separating the rhombohedral and tetragonal phases, similar to that in PZT.²⁸ The structure of these MPB's was first considered to be a mixing of the two adjacent ferroelectric phases.^{28–31} However, the recent experimental discovery of a monoclinic phase in PZT (Refs. 32–34) at the MPB has completely changed this picture. A key feature of this structure is that the polarization vector is no longer constrained to lie along a symmetry axis, as in the rhombohedral and tetragonal structures, but instead can rotate within a monoclinic plane. The presence of the monoclinic phase in PZT is not a peculiarity of this system^{34–36} and is also present in PMN-PT and PZN-PT, but instead of a Cm phase as in PZT, a Pm one^{37–40} is observed in these relaxor-PT systems. Nevertheless, depending on the history (temperature and cooling process) there is still an ambiguity since an orthorhombic phase was also been reported.^{40–42}

These experimental results have received theoretical support from a first-principles-derived approach which predicts stability and properties of MPB piezocrystals.⁴³ Indeed in a compositionally homogeneous approximation, only the rhombohedral and tetragonal phases were predicted to be stable at the MPB, as conventionally believed. However, when an on-site alloying self-energy term (up to fourth power) is considered in the free energy, a monoclinic state is stabilized and effectively bridges the rhombohedral and tetragonal states.⁴⁴ It is important to emphasize that the alloying self-energy term is considered within a random-field approximation and therefore should be significantly affected⁴⁵ when one deals with a relaxor of the 1:2 or 1:1 type. Furthermore, it was found that an eighth-order Devonshire expansion generates monoclinic ferroelectric states and even triclinic phases can be obtained from a 12th-order expansion of the free energy.⁴⁶

In the present work the first experimental evidence of a monoclinic phase in a 1:1-type relaxor-PT system, namely, PSN-PT, is reported and a new phase diagram is obtained. Theoretical analysis based on first-principles calculations have been performed also on the MPB region and bears out the existence of the monoclinic state in such a system. Competing orderings of the polarization along multiple directions on a mesoscale are found to play a key role and explain the

crossing from rhombohedral to tetragonal phases through this monoclinic phase.

II. EXPERIMENTAL AND THEORETICAL METHODS

PSN-PT samples with $x=0.26, 0.37, 0.40, 0.43, 0.45, 0.50$, and 0.55 were prepared by conventional solid-state reaction using high-purity (better than 99.9%) lead oxide, scandium oxide, niobium oxide, and titanium oxide as starting compounds. After mixing in stoichiometric proportions without using any excess $[\text{Nb}_2\text{O}_5, ^{47,48} \text{Fe}_2\text{O}_3 \text{ (Ref. 49)}]$, powders were first calcined at 1250 °C for 2 h 30 min, uniaxial cold pressed, and sintered at 1280 °C for 3 h. Precautions (covered crucible and PbO-rich atmosphere) have been taken to avoid PbO losses during the calcination and sintering processes. At the close of this procedure, we obtained a pure perovskite phase of PSN-PT free from the parasitic pyrochlore phase. An investigation of the microstructure using a scanning electron microscope [(SEM) FEG, LEO 1530] of the ceramics did not reveal the presence of an intergranular second phase. The mean size of the grain is about 8 μm . In addition, energy dispersion scanning showed a homogeneous cationic distribution from one grain to another. Ceramic samples were polished and cleaned, and sputtered-gold electrodes were applied. To eliminate strains caused by polishing, samples were annealed in air at 700 °C for 1 h and then slow cooled. The temperature dependence of the dielectric constant was measured at various frequencies in a temperature range from 290 to 800 K using a Hewlett-Packard 4192A impedance analyzer and a furnace with an estimated precision of 2 K. X-ray-diffraction measurements were performed on a high accuracy, two-axis diffractometer in a Bragg-Brentano geometry using $\text{Cu-K}\beta$ wavelength issued from a 18-kW rotating anode generator with diffraction angle precision better than 0.002° (2θ). The data were collected in two parts, first in a N_2 flow cryostat from 90 to 295 K (precision better than 0.1 K) and then in a furnace from 295 to 800 K (estimated precision of 2 K). Selected regions of the diffractogram, containing the (200), (220), and (222) pseudocubic reflections, were recorded. Because of complicated peak shapes, a very careful peak-fitting analysis was realized using PROFILE software (V1.30 Socabim) to take into account factors such as asymmetry and mixing phases. For each selected region the peak positions were determined and when it was possible, the lattice parameters were obtained from a fit of several reflections. The neutron powder-diffraction pattern was collected at 8 K on a 3T2 high-resolution goniometer on a thermal source ($\lambda=1.227 \text{ \AA}$) using the Orphée reactor facilities at Laboratoire Léon Brillouin (Saclay, France). Structural Rietveld refinements on both x-ray and neutron patterns were carried out with XND software.⁵⁰

Concerning the theoretical method, we used the computational scheme proposed in Ref. 51 for the $[\text{Pb}(\text{Sc}_{0.5}\text{Nb}_{0.5})\text{O}_3]_{1-x}(\text{PbTiO}_3)_x$ alloy. This scheme is a generalization of the first-principles-derived alloy effective Hamiltonian approach of Refs. 43 and 52—which was developed for solid solutions having two different kinds of B atoms. Conceptually, the generalization to the study of

PSN-PT consists of including on-site and intersite alloying effects via two perturbations over the five-atom $\text{Pb}\langle B'\rangle\text{O}_3$ system, in which the $\langle B'\rangle$ atom is a virtual atom involving a kind of potential average among the Sc, Ti, and Nb atoms.⁵³ The first perturbation breaks the virtual $\langle B'\rangle$ atom into the (true) Ti atom and a virtual $\langle B''\rangle$ atom, in which $\langle B''\rangle$ involves a potential average between the Sc and Nb atoms. The second perturbation then leads to the existence of the true Sc and Nb atoms from this $\langle B''\rangle$ atom. The parameters entering the analytical expression of the total energy for the alloy effective Hamiltonian of $[\text{Pb}(\text{Sc}_{0.5}\text{Nb}_{0.5})\text{O}_3]_{0.50}(\text{PbTiO}_3)_{0.50}$, i.e., for PSN-PT with 50% of Ti atoms occupying the B sites, are determined by performing first-principles calculations^{54,55} on small cells. In principle, all the parameters in the alloy effective Hamiltonian should change when one varies the composition x in the $[\text{Pb}(\text{Sc}_{0.5}\text{Nb}_{0.5})\text{O}_3]_{1-x}(\text{PbTiO}_3)_x$ solid solution. However, we numerically found that only some parameters, namely, the ones denoted B_{1yy} , B_{4yz} , $Q_{|j-i|}$, and $R_{|j-i|}$ in Ref. 56 significantly change between $x=0.50$ and 0.40 . The composition dependence of these parameters is assumed to be linear, and is determined by performing first-principles simulations on cells with two different compositions, namely, $x=0.50$ and 0.40 . Such a linear composition-dependence approach is only realistic when exploring a narrow range of compositions around $x=0.50$. Consequently, theoretical results can (most likely) “only” be compared with the present experimental data for the samples with $x=0.40, 0.43, 0.45, 0.50$, and 0.55 . Conversely, comparing our predictions resulting from this numerical scheme with our measurements for the Ti-poorest grown samples—for which $x=0.26$ and 0.37 —is (very likely) inappropriate. That is the reason why we limit our calculations to Ti concentrations ranging between 0.40 and 0.55 .

Once our effective Hamiltonian is fully specified, its energy is then used in Monte Carlo simulations on large (typically $12\times 12\times 12$ or $16\times 16\times 16$) supercells, mimicking the disordered structures under investigation. The outputs of Monte Carlo procedure are the polar local soft mode \mathbf{u} and the homogeneous strain tensor η . The \mathbf{u} soft mode is directly related to the electrical polarization, while η provides information about the crystallographic system.

III. EXPERIMENTAL AND THEORETICAL RESULTS

A. Dielectric study

Since the pioneering work of Tennery, Hang, and Novak,²⁶ no study of the dielectric and structural properties of the whole phase diagram of the PSN-PT system has been reported, to the best of our knowledge. Only a few articles were focused around the concentration of PSN-PT of 43% in order to optimize the electromechanical properties by appropriate doping^{47–49} since the high piezoelectric response is associated with the MPB. From our samples we obtained a “bell” shape in the maximum of the dielectric constant as a function of PT concentration (Fig. 1) confirming the MPB is localized near 43%. For each composition, only one anomaly is observed and a deviation from a Curie-Weiss law is evidenced above T_{max} , the temperature of the maximum of the

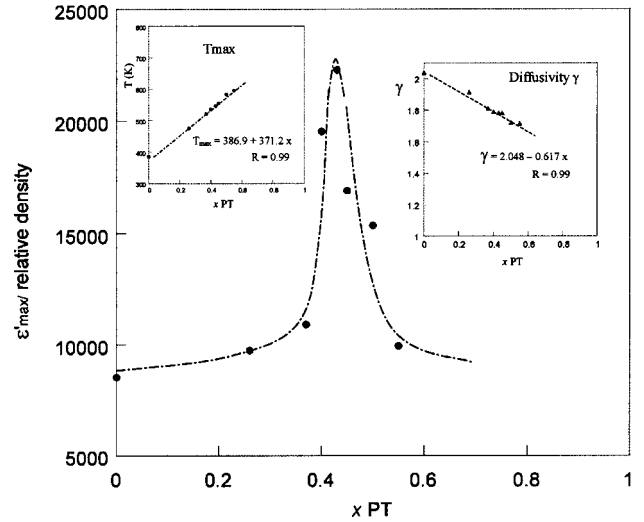


FIG. 1. $\epsilon'_{\text{max}}/\text{relative density}$ vs PT concentration (data for $f = 10$ kHz). The dielectric constant has been divided by the relative density of the ceramic to rule out this extrinsic effect on the dielectric value. Inset: T_{max} vs PT and γ vs PT, respectively, obtained from a modified Curie-Weiss law fit; for pure PSN we used our data from Ref. 16.

dielectric constant, and a modified law, i.e., $1/\epsilon - 1/\epsilon_{\text{max}} = \alpha(T - T_{\text{max}})^\gamma$ is preferred to take this deviation into account. ϵ_{max} is the maximum of the dielectric constant at a given frequency and γ is the critical exponent ranging between $\gamma = 1$ for conventional ferroelectrics and $\gamma = 2$ for lead-based relaxors.⁵⁷ When $\gamma = 1$ the constant α is equal to $1/C$, where C is the Curie constant and $T_{\text{max}} = T_0$ is the Curie temperature.

As expected, T_{max} increases and γ decreases with increasing PT content (inset, Fig. 1). These variations can be fitted by a linear law $T_{\text{max}} = T_{\text{max}}^{\text{PSN}} + ax_{\text{PT}}$ and $\gamma = \gamma^{\text{PSN}} - bx_{\text{PT}}$ ($a = 384.1$, $b = -0.007$), which reflects the progressive change from PSN relaxor to PT ferroelectric behavior.

B. Structural study

Figure 2 shows the experimental x-ray-diffraction patterns of the pseudocubic (200) Bragg reflection at $T = 300$ K for PSN-PT with $0.26 \leq x \leq 0.55$. As x increases, the average symmetry gradually changes from rhombohedral to tetragonal, indicated by a pronounced splitting. For $x = 0.26$ and 0.55 , the diffraction peaks are well defined and the symmetry is unambiguously rhombohedral and tetragonal, respectively, whereas the intermediate compositions give more complicated diffraction patterns. Different scenarios can be used to describe this situation: (i) mixing phases between the rhombohedral Ti-poor concentration and the tetragonal Ti-rich concentration regions, (ii) a phase coexistence between the cubic high-temperature phase and the tetragonal low-temperature phase due to metastable states associated to a first-order phase transition, and (iii) appearance of a new low-symmetry phase (orthorhombic, monoclinic, triclinic).

1. Rhombohedral phase for $x \leq 0.26$

For $x \leq 0.26$, a rhombohedral phase is stable as characterized by the singlet (200)_r for $x = 0.26$ (Fig. 2). The results of

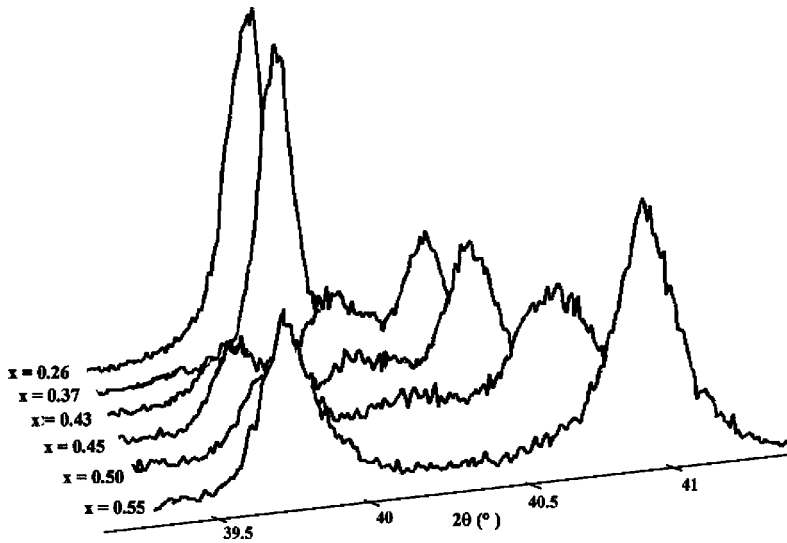


FIG. 2. X-ray-diffraction patterns of the pseudocubic (200) Bragg reflection at $T=300$ K for PSN-PT with $0.26 \leq x \leq 0.55$.

the temperature-dependence studies for $x=0.26$ are presented in Fig. 3. The structural phase transition from cubic to rhombohedral occurs at $T_c=480(5)$ K with no detectable discontinuity. The observed diffraction peaks showed no evidence of any additional phase transitions and/or phase coexistence, and the structure remains rhombohedral down to the lower temperature.

At $T=295$ K, a detailed structural investigation by means of an x-ray Rietveld analysis (Table I) confirmed the rhombohedral phase with an $R3m$ space group, since quite good reliability factors ($R_{wp}=8.94\%$, $R_B=3.06\%$, $GOF=1.33$) were obtained. Because of the weaker contribution of light atoms compared to heavy ones, such as Pb or Nb, to the x-ray-diffraction pattern, the large temperature factors for oxygen were fixed in the refinement to the value classically obtained from neutron diffraction in lead-based perovskites. The cell parameters at $T=295$ K are $a_r=4.0403$ Å and $\alpha=89.85^\circ$, and atoms are found to be displaced from the cubic special positions in the same way as pure PSN:Pb and Sc/Nb/Ti ions are shifted by 0.30 and 0.15 Å from their ideal position, respectively, along the $[111]$ polar axis, giving rise

to a polarization $P=47 \mu\text{C}/\text{cm}^2$, which is higher than the polarization of pure PSN (Ref. 16) ($P=33 \mu\text{C}/\text{cm}^2$).

The lead thermal parameter was found as large (1.92 Å^2) as usual in the lead perovskite and is a strong indication of possible disorder.⁵⁸ In addition to the cooperative shift of 0.30 Å for the Pb atom along the polar $[111]$ axis, we have tested disordered shifts with directions perpendicular to the polar axis, accordingly to the procedure now classically used in these compounds.^{9,16} The Pb atom shifts from its position, which improves the refinement ($R_{wp}=8.78\%$) when Pb is displaced about 0.2 Å perpendicular to the polar axis (inset, Fig. 3). In this minimum, the B_{Pb} thermal factor recovers to a normal value of $B_{\text{Pb}}=0.86 \text{ Å}^2$. The composition of cooperative shifts along the $[111]$ polar direction with disordered (short-range) shifts along $[-1-12]$ gives the local position of the lead atom inside the rhombohedral cell, which is very close to the $[001]$ pseudocubic direction.

2. Tetragonal phase for $x \geq 0.55$

The evolution of the lattice parameters with temperature is illustrated on Fig. 4. With decreasing temperature, the tetragonal phase appears through a weak first-order transition at $T_c=590(5)$ K and the tetragonal distortion can be observed increasing the ratio c_t/a_t until 1.035 at $T=90$ K without the appearance of any other phase. The effects of $\text{Sc}^{3+}/\text{Nb}^{5+}$ substitution on the tetragonal phase compared to pure PbTiO_3 include a decrease of the tetragonal ratio c_t/a_t and a softening of the cubic-tetragonal order phase transition. The results of the detailed x-ray Rietveld analysis of the 295-K tetragonal structure are summarized in Table I. The space group used in this refinement is that of PbTiO_3 , i.e., $P4mm$ ($R_{wp}=7.76\%$, $R_B=2.61\%$, $Gof=1.55$). Pb and Sc/Nb/Ti ions are shifted of 0.37 and 0.24 Å, respectively, along the $[001]$ polar axis giving rise to a polarization of $P=67 \mu\text{C}/\text{cm}^2$, which is smaller than the PbTiO_3 one⁵⁹ ($P=90 \mu\text{C}/\text{cm}^2$). Tests of additional disorder of the Pb atom did not improve the refinement, supporting the observation of a normal value for the Pb thermal parameter B_{Pb}

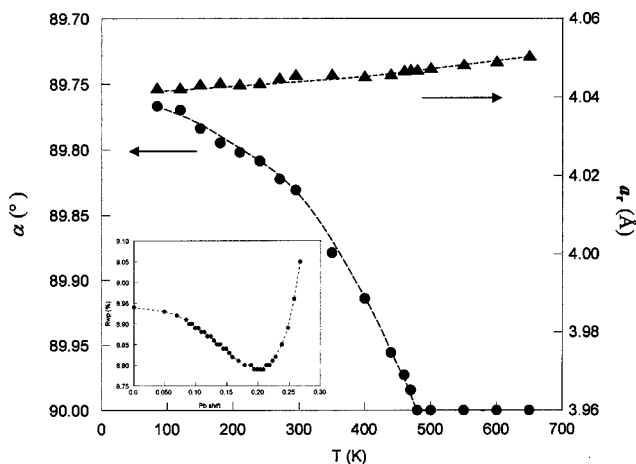


FIG. 3. Cell parameter evolution as a function of temperature in $x=0.26$. Inset: R_{wp} as a function of Pb shift along the $[-1-12]$ direction perpendicular to the $[111]$ polar axis at room temperature.

TABLE I. Rietveld analysis results using x-ray patterns at room temperature for $x=0.26$ and 0.55 compared to pure PSN (Ref. 16) and pure PbTiO_3 .⁵⁹

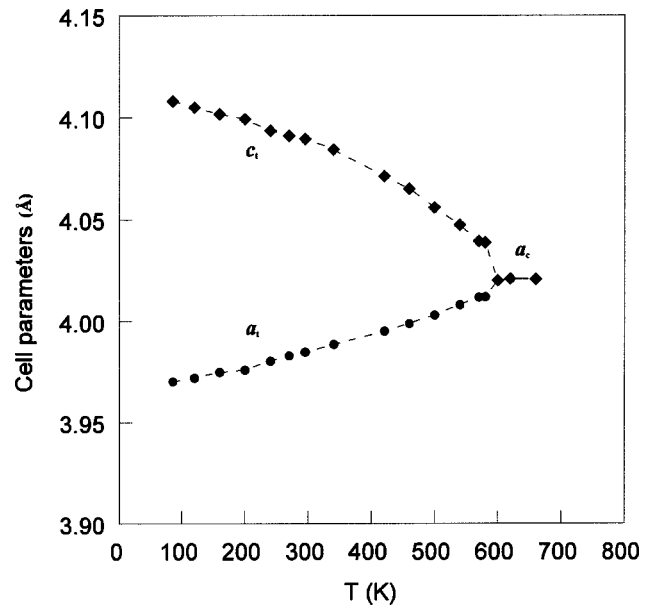
		PSN ^a ($x=0$) 300 K $R3m$ Neutrons	PSN _{0.74} -PT _{0.26} ($x=0.26$) 295 K $R3m$ RX	PSN _{0.45} -PT _{0.55} ($x=0.55$) 295 K $P4mm$ RX	PT ^b ($x=1$) 300 K $P4mm$ Neutrons
Lattice parameters	a (Å)	4.0704(1)	4.0403(1)	3.9773(1)	3.902(3)
	c (Å)			4.0835(1)	4.156(3)
	α (°)	89.94(5)	89.854(3)	90	90
Position of Pb	$x\ x\ x$	0	0	0	0
$B_{\text{eq(Pb)}} (\text{Å}^2)$		2.25(7)	1.92	0.95	
Position of O	x	0.5427(11)	0.5406(16)	0.5	0.5
	y	0.5427(11)	0.5406(16)	0	0
	z	0.0358(11)	0.0478(23)	0.5947(17)	0.6174(3)
$B_{\text{eq(O)}} (\text{Å}^2)$		1.80(7)	1.70	1.70(0)	
Position of O	x			0.5	0.5
	y			0.5	0.5
	z			0.0858(24)	0.1118(3)
$B_{\text{eq(O)}} (\text{Å}^2)$				1.70(0)	
Position of Sc/Nb/Ti	$x\ x$	0.5310(5)	0.5218(3)	0.5	0.5
	z	0.5310(5)	0.5218(3)	0.5324(6)	0.5377(4)
$B_{\text{eq(Sc/Nb/Ti)}} (\text{Å}^2)$		0.63(5)	0.27(0)	0.27(0)	
$\delta_{\text{Pb-O}} (\text{Å})$		0.28(4)	0.30(4)	0.37(5)	0.49(4)
$\delta_{\text{Sc/Nb/Ti-O}} (\text{Å})$		0.07(6)	0.15(3)	0.24(4)	0.31(5)
Polarization P ($\mu\text{C}/\text{cm}^2$)		33	47	67	90
	R_{wp} (%)	5.49	8.94	7.76	2.50
	R_{exp} (%)	3.35	6.72	5.00	
	Gof	1.64	1.33	1.55	
	R_{Bragg} (%)	3.18	3.06	2.61	

^aReference 16.^bReference 59.

$=0.97 \text{ Å}^2$, which is comparable to the value obtained in the rhombohedral PSN-PT by 26% when the Pb shift was added ($B_{\text{Pb}}=0.86 \text{ Å}^2$) (see above).

3. Monoclinic phase for $0.26 < x < 0.55$

Due to the complicated diffraction patterns of the intermediate composition $0.26 < x < 0.55$ (Fig. 2), we have focused the description of our results on the concentration $x=0.43$ because of its optimized piezoelectric responses. For this composition, a supplementary peak is clearly observed between $(200)_t$ and $(002)_t$ tetragonal peaks [Figs. 2 and 5(a)]. These three peaks are somewhat broader but otherwise well resolved and their 2θ positions as a function of temperature are plotted in Fig. 5(b). When decreasing temperature from ~ 680 K, the splitting of the $(200)_c$ cubic Bragg peak occurs at $T_{c1}=540(5)$ K into $(200)_t$ and $(002)_t$ reflections, unambiguously indicating a tetragonal symmetry. The tetragonal strain c_t/a_t increases when temperature decreases from T_{c1} to a value of 1.010 at $T_{c2}=440(5)$ K, below which a third peak appears [peak (2) in Fig. 5(a)]. As the temperature continues to decrease, the full width at half maximum (FWHM) [Fig. 5(c)] and the intensity of this supplementary

FIG. 4. Cell parameter evolution as a function of temperature for $x=0.55$.

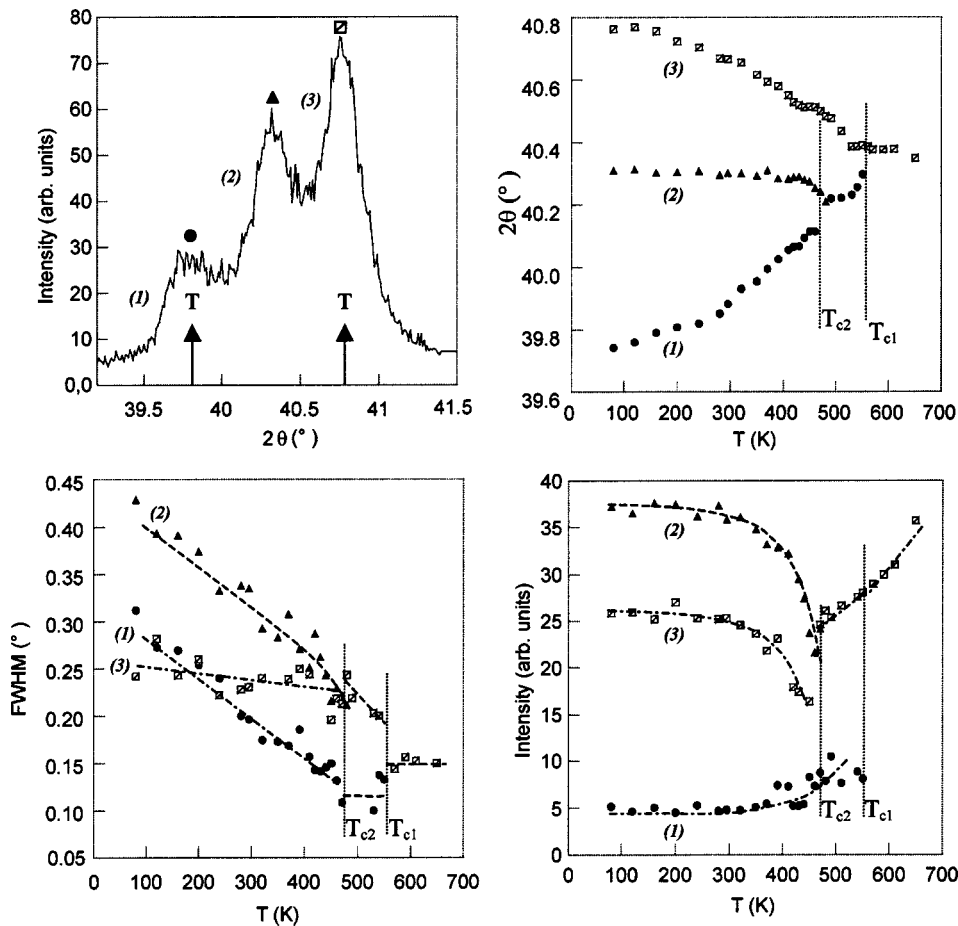


FIG. 5. (a) Selected pattern area around the (200) pseudocubic reflection for $x=0.43$ at $T=120$ K; (b) 2θ position of (200) pseudocubic reflections; (c) temperature dependence of FWHM; (d) intensities of (200) pseudocubic reflections.

peak increase [Fig. 5(d)]. Such work had also been done (but results are not given in this paper) for all other peaks, in particular, (220) and (222) pseudocubic reflections.

Analysis of these temperature evolutions allows to exclude two of the three scenarios mentioned above: first, a mixing between the tetragonal phase and a rhombohedral phase cannot be considered because the FWHM of the peak (2) increases when the temperature decreases [Fig. 5(d)], instead of being constant or diminishing when temperature decreases, as expected if this peak was associated with a low-temperature rhombohedral phase; second, a mixing of the residual trapped cubic phase with the tetragonal phase cannot be considered either since a strong increase of the intensity of the peak (2) with decreasing temperature is observed, which rules out its possible association with the high-temperature cubic phase.

The broadening and increase of intensity of the third peak can only be explained by the appearance of a new phase different from a rhombohedral one. This new phase appears to the detriment of the tetragonal phase but there is coexistence of both those phases down to the lowest temperature. Indeed, a sole phase is not enough to take into account the set of all diffraction patterns [(200), (220), and (222) pseudocubic reflections].

The same type of x-ray patterns such as those in Fig. 5(a) have been found in PZN-PT (Ref. 42), which the authors conclude to be an orthorhombic phase (mixed with a small amount of residual tetragonal one) from consideration of the

splitting and relative intensities of the diffraction profiles at a given temperature. However, thanks to the complete temperature evolution the hypothesis of an orthorhombic phase mixed with a tetragonal phase cannot be considered from our result. Indeed in this hypothesis, the high (2) peak, i.e., peak (3), includes both the $(020)_o$ orthorhombic reflection and the $(200)_t$ tetragonal one, whereas peak (2) contains the $(202)_o$ orthorhombic one. Then when temperature is decreased, one should expect a broadening for peak (3) whereas peak (2) should have its FWHM constant, which is not what is observed experimentally [Fig. 5(c)]. Our results indicate a lower symmetry, and a phase with at least a monoclinic symmetry is needed to account for our data.

In order to go further, we have performed a detailed Rietveld analysis of the structure from the full pattern obtained by neutron diffraction, at low temperature ($T=8$ K). In this study anisotropic profiles were introduced as in the studies of PZN-PT (Refs. 33 and 37) and of PMN-PT,³⁷ which are probably originated from the anisotropic shape of the ferroelectric domains observed by optical measurements in PZN-PT (Ref. 35) and/or the coexistence with the tetragonal phase (size effects and internal stress fields). We have proceeded in several steps in order to test many possible structural models. At first, we have considered the existence of a sole low-symmetry phase (monoclinic Pm and Cm , triclinic $P1$) but poor agreement was obtained ($R_{wp} \approx 15\%$). A tetragonal phase was then added to improve the refinement. From these refinements, we have definitively excluded the

TABLE II. Result of the Rietveld neutron-diffraction refinements on $x=0.43$ at $T=8$ K.

Solution $X + P4mm$		$Cm + P4mm$	$Pm + P4mm$
R_{wp}		4.92	4.84
R_{Bragg}		3.47	3.37
GoF		1.42	1.39
% phase X		61	85
% phase $P4mm$		39	15
X phase			
Lattice parameters	a (Å)	5.7534(10)	4.0370(6)
	b (Å)	5.7085(10)	4.0100(6)
	c (Å)	4.0152(9)	4.0677(6)
	α (°)	90.00	90.00
	β (°)	90.26(2)	90.38(1)
	γ (°)	90.00	90.00
	B_{eq} (Å ²)	1.25(5)	1.60(5)
Position of Pb	$x x x$	0 0 0	0 0 0
	B_{eq} (Å ²)	1.25(5)	1.60(5)
	B_{eq} (Å ²)	1.25(5)	1.60(5)
Position of O	x	0.4101(12)	0.5687(24)
	y	0	0
	z	0.0416(30)	0.4099(25)
	B_{eq} (Å ²)	0.10(3)	0.92(12)
Position of O	x	0.1905(21)	0.0546(16)
	y	0.2469(11)	0.5
	z	0.5010(28)	0.4192(22)
	B_{eq} (Å ²)	0.64(5)	0.14(11)
Position of O	x		0.5611(24)
	y		0.5
	z		-0.067(17)
	B_{eq} (Å ²)		1.15(14)
Position of Sc/Nb/Ti	x	0.4538(9)	0.5277(21)
	y	0	0.5
	z	0.5215(27)	0.4418(14)
	B_{eq} (Å ²)	0.32(8)	0.12(10)
$P4mm$ phase			
Lattice parameters	a (Å)	4.0047(4)	4.0027(3)
	c (Å)	4.0960(6)	4.1009(5)
Position of Pb	$x x x$	0 0 0	0 0 0
Position of O	x	0.5	0.5
	y	0	0
	z	0.4720(4)	0.4650(4)
Position of O	$x y$	0.5	0.5
	z	0.0853(14)	0.0866(11)
Position of Sc/Nb/Ti	$x x$	0.5	0.5
	z	0.5327(16)	0.5319(10)

existence of the mixing of rhombohedral, orthorhombic, and triclinic phases ($R_{wp} > 5\%$). Clearly the best refinement is obtained with a monoclinic phase (Table II).

Nevertheless it is not possible to assign a space group to this new phase, i.e., to distinguish between Cm and Pm space groups, since both structural models give very close agreement factors. In both solutions there is a strong amount of tetragonal phase: $\sim 39\%$ with Cm and $\sim 15\%$ with Pm , as

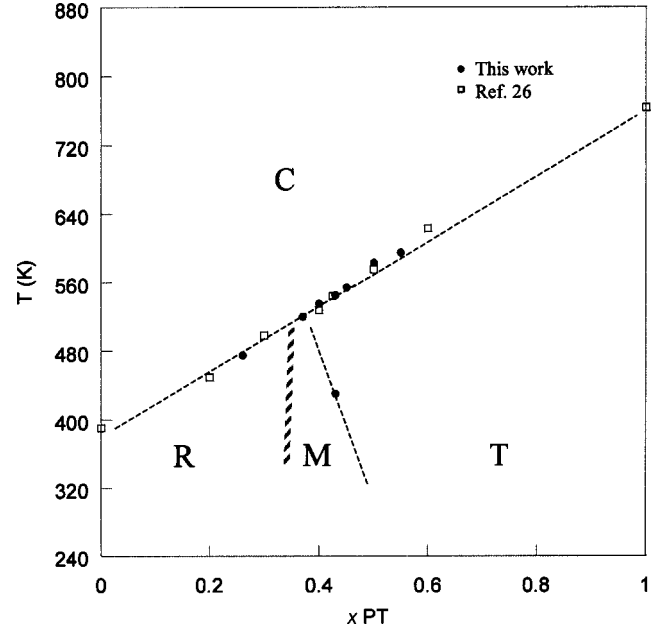


FIG. 6. Structural phase diagram of PSN-PT system.

deduced from the scale factor ratio of the fitting. To settle between Pm and Cm space groups, one should manage to eliminate or at least significantly diminish this tetragonal phase in order to reduce the parameters to be refined. Most probably a small grain size and/or internal microstrains⁴⁰ induce a change in the competition and modify the ground state. In particular, these effects probably explain the strong amount of tetragonal phase that we obtained in our refinement. Nevertheless, a composition fluctuation is not excluded and can be superimposed to the grain-size effect. Further analysis to conclude on the type of monoclinic space group is now in progress, but nevertheless we can put forward that the ground state of PSN-PT (43%) is of a monoclinic symmetry.

C. Theoretical study

In order to gain further insight into the structural properties of PSN-PT near its morphotropic phase boundary, we performed some finite-temperature simulations for samples with Ti compositions ranging between 0.40 and 0.55. Our alloy effective Hamiltonian approach predicts that disordered PSN-PT with $x=0.50$ exhibits a paraelectric cubic state at high temperature and a low-temperature ferroelectric $4mm$ tetragonal phase for which the total polarization lies along the $\langle 001 \rangle$ pseudocubic direction. These findings are consistent with the experimental results displayed in Fig. 6. The theoretical paraelectric-ferroelectric phase transition occurs around 660 K, which compares rather well with the present experimental value ≈ 585 K.

Another direct comparison between our predictions and our measurements can be made for the PSN-PT solid solutions exhibiting 55% of Ti atoms among their B sites. The calculations yield a tetragonal system with an axial ratio c_t/a_t of 1.030 at room temperature, which is in excellent agreement with the measured value around 1.027 (see Table

I). For this temperature and for this alloy, the theoretical ferroelectric-induced internal atomic displacements with respect to the ideal cubic positions are 0.0931 ± 0.0008 , 0.0723 ± 0.0007 , and 0.0321 ± 0.0003 for the two kinds of oxygen atom and the averaged B atom, respectively, when adopting the convention that the Pb displacement is equal to zero. These three predicated values agree very well with the corresponding experimental results of 0.0947 ± 0.0017 , 0.0858 ± 0.0024 , and 0.0324 ± 0.0006 displayed in Table I.

Our simulations further predict that the mimicked solid solution exhibiting the smallest Ti composition, namely, PSN-PT with 40% of Ti, is rhombohedral at low temperature as well as at room temperature. This result is consistent with the experimental finding that the phases bordering the MPB in PSN-PT are rhombohedral for small Ti compositions and tetragonal for larger Ti concentrations. However, the exact compositions delimiting this MPB are very likely strongly dependent on the Helf parameters as emphasized in Ref. 56. As a result, it is possible that the “true” PSN-PT with 40% of Ti is slightly inside the MPB—as the experimental results depicted in Fig. 2 tend to indicate—rather than slightly outside the MPB, as our calculation predicts. Furthermore, room-temperature calculations for a Ti concentration of 40% yield a rhombohedral angle of 89.79° . They also yield ferroelectric-induced internal displacements of 0.0403 ± 0.0049 and 0.0313 ± 0.0038 for the Cartesian components of the oxygen atoms and of 0.0139 ± 0.0017 for the averaged B atom, when imposing, once again, that the Pb displacement is null. These predicted rhombohedral angle and atomic displacements are thus rather consistent with an extrapolation (up to a Ti concentration of 40%) of the experimental data of PSN-PT, with 26% Ti, that are displayed in Table I.

We now focus on compositions lying inside the “theoretical” MPB. More precisely, we first generate a large ($16 \times 16 \times 16$) alloy configuration mimicking a disordered PSN-PT solid solution with a Ti composition of 41.6%. Performing simulations at 50 K for this configuration yields a polar local soft mode \mathbf{u} whose Cartesian components, in atomic units, are $(0.003 \pm 0.003, 0.014 \pm 0.003, \text{ and } 0.0732 \pm 0.001)$ (note that we use the convention that the x , y , and z axes are chosen along the pseudocubic $[100]$, $[010]$, and $[001]$ directions, respectively). In other words, the corresponding polarization can be statistically considered to lie along a $\langle 0uv \rangle$ direction, with $0 < u < v$. The resulting phase is thus a monoclinic symmetry with a Pm space group. Interestingly, generating another $16 \times 16 \times 16$ random alloy configuration with the same Ti composition of 41.6% also leads to a monoclinic phase at 50 K. However, this phase has a Cm space group since its polarization lies along a $\langle uuv \rangle$ direction, with $0 < u < v$. The corresponding polar soft mode \mathbf{u} is predicted to have the following Cartesian components, in atomic units: $(0.006 \pm 0.002, 0.006 \pm 0.002, 0.0741 \pm 0.001)$. Similarly, we found that some PSN-PT alloy configurations associated with a slightly smaller Ti composition, namely, 41.4%, adopt a monoclinic Cm space group. The corresponding local polar mode is $(0.030, 0.030, 0.062)$, i.e., it has Cartesian coordinates that are closer to each other than those associated with the local polar modes at a Ti concentration of 41.6%. This indicates that the polarization rotates

from the pseudocubic $[001]$ direction to the pseudocubic $[111]$ direction as the Ti composition decreases in the MPB area of PSN-PT, or equivalently, that the monoclinic phases indeed act as a structural bridge between the tetragonal and rhombohedral structures delimiting the MPB. Our theoretical results thus point out that (i) there are intermediate monoclinic phases in the MPB of PSN-PT, (ii) the monoclinic phases associated with Pm and Cm space groups are very close to each other in the free-energy space, and (iii) a minor change of atomic distribution and/or a slight modification in composition is enough to alter the space group of the monoclinic ground state. Furthermore, the nonstoichiometry, or equivalently, the short-range order, may affect the range of the monoclinic phase. Features (i)–(iii) are all consistent with the present experimental findings. Furthermore, features (ii) and (iii) make the MPB of PSN-PT rather unique.

IV. DISCUSSION AND CONCLUSION

The true origin of the relaxor behavior as observed in the PSN-PT system remains open. Recently, Blic *et al.* have proposed to explain relaxor features with the use of a spherical random bond random-field model,^{60,61} which incorporates the previous models, the dipole glass (random bond) one,⁴ and the random-field (or pinning) one³ in a self-consistent manner. In this hybrid model, the dynamics of the polarization is controlled by the random/spherical bond characteristics, which are induced by random fields. Multiple competing orderings of the polarization along multiple directions are allowed. Such an approach allows sophisticated understanding of competing interactions on the mesoscale. Very recently,⁶² density-functional theory calculations performed on PZT have shown that the distortions of the material away from the parent perovskite structure can be predicted from the local arrangement of the Zr and Ti cations. The Pb shifts in directions are sensitive to the B-cation environment. Pb shifts are toward Ti neighbors and away from Zr neighbors.

We believe that our structural study of PSN-PT is helpful for understanding relaxor behavior by obtaining an atomic level picture of competing interactions. In particular, our study of the structural evolution of PSN-PT allows us to propose a phase diagram (Fig. 6) that is very similar to the phase diagrams of 1:2 compounds PMN-PT and PZN-PT.

The analysis performed on PSN-PT of 26% has shown that the stable ground state is similar to that of pure PSN,¹⁶ i.e., the structure is of a rhombohedral symmetry with a macroscopic polar axis oriented along the $[111]$ direction. In this structure, Pb and O are locally displaced from their ideal positions in the perovskite unit cell along the polar $[111]$ direction. Moreover analysis of the B thermal parameters reveals similar features already reported in pure PSN (Refs. 16 and 58) or $\text{PbSc}_{1/2}\text{Ta}_{1/2}\text{O}_3$,⁶³ but also in mixed systems such as PZT (Refs. 64 and 65) and in PMN-PT.^{9,37} In particular, we have observed additional disordered displacement for lead atoms inside the rhombohedral phase along the $[001]$ local tetragonal distortion, in agreement with Ref. 62, which shows that $\langle 100 \rangle$, $\langle 211 \rangle$, or $\langle 110 \rangle$ Pb shifts are preferred over $\langle 111 \rangle$, even in rhombohedral phase where the overall polarization is along $[111]$.

Therefore the global physical picture of PSN-PT appears to be similar to that observed in PMN-PT and PZT, in which competition between rhombohedral and tetragonal orders occurs. In the Ti-poor region of the phase diagram the rhombohedral phase is the ground state but local monoclinic order is detected mainly due to the lead atoms. Indeed, lone pair electrons in Pb results in formation of short Pb-O bonds comparable to those obtained in PT (Ref. 59) or PbO (Refs. 65 and 66) and gives rise to strong Pb polarizability. In the Ti-rich region the microscopic physics underlying the low-temperature phase of the end-point PT is well known. Indeed the ground-state structure has shifts along [001] with a strong lattice strain that stabilizes this direction. A rhombohedral ferroelectric phase with [111] shifts is not favored and does not occur because of the large electronic hybridization between Pb and O, as may be seen by comparison with BaTiO₃, which has a rhombohedral ferroelectric ground state. As a result both Ti and Pb are strongly displaced, giving rise to strong ferroelectricity in PT. The consequence of Ti substitution by Sc/Nb from pure PT is a destabilization of the Ti [001] direction against a Sc/Nb [111] direction.

Between the two regions, the Ti-poor and the Ti-rich ones, an intermediate monoclinic ground state is stabilized and “bridges” the rhombohedral and the tetragonal phases in total agreement with our theoretical simulations. The monoclinic phase has been evidenced on PSN-PT of 43% from two different analyses, i.e., X-ray profile analysis and Rietveld neutron powder refinement. Nevertheless, it is very difficult to identify any space group. Indeed, theoretical results indicate that *Pm* and *Cm* monoclinic space groups are very close to each other in free-energy space so a minor change of atomic distribution and/or modification of composition is enough to alter the space group of the monoclinic ground state.

Besides, our results suggest that the “bridge” through the monoclinic state is not a narrow concentration range: a gradual transformation from the rhombohedral to the tetragonal state takes place. Indeed inside the rhombohedral phase lead atoms are locally shifted along [001] direction, whereas *B* cations are shifted along [111], which reconstructs a local monoclinic symmetry within the macroscopic rhombohedral state of PSN-PT $x \leq 26\%$. When doping with Ti, the coher-

ence length of this monoclinic short-range region increases up to a long-range monoclinic state for $x = 43\%$. When the Ti content continues to increase, the monoclinic ground state is destroyed in favor of a tetragonal phase such as in PSN-PT of 55%, similar to that of pure PT. These results show that the relative amount of Sc/Nb/Ti influences the ground state and especially the local structure in which Pb atoms are disordered, in agreement with Ref. 62, which demonstrates that the Pb local directions are very sensitive to the local environment imposed by the *B*-cation neighborhoods.

Our results have shown that in this 1:1-type relaxor-based compound a monoclinic ground state exists in the MPB region. In particular, like in PZN-PT and PMN-PT, it is probable that a strong enough electric field,⁶⁷ a small grain size, and/or internal microstrains⁶⁸ should induce change in the competition and significantly modify the direction of polarization and ground states.

The monoclinic phase is not a direct consequence of a mixing between any relaxor and PT as in the case of PbFe_{2/3}W_{1/3}O₃-PbTiO₃,⁶⁹ where the possibility of such a phase has been definitely rejected. Instead, a monoclinic state can be stabilized if a peculiar arrangement between different heterovalent ions is obtained. The random fields due to Sc³⁺ and Nb⁵⁺ arrangements in disordered pure PSN are not enough to stabilize the monoclinic state,⁵² but modifications of these random fields by Ti⁴⁺ substitution induce such a symmetry. The random fields in the case of the PSN relaxor can also be modified by appropriate thermal treatment, as ordering or disordering of Sc/Nb cations can be induced. Preliminary results on PSN-PT of 43% have already been obtained showing the implication of the order degree (or random fields) on the electrical properties and on the structural ground state, and a complete study, both experimental and theoretical, is under investigation.

ACKNOWLEDGMENTS

The theoretical part of this work was supported by ONR Grant Nos. N00014-01-1-0365 and N00014-01-1-0600, and NSF Grant No. DMR-9983678. The authors are grateful to J. Chevreul and M. Gramond for helping during x-ray-diffraction experiments and electrical measurements.

¹L. E. Cross, *Ferroelectrics* **76**, 241 (1987).

²G. A. Smolenskii, V. A. Isupov, A. I. Agranoskaya, and S. N. Popov, *Sov. Phys. Solid State* **2**, 2584 (1961).

³W. Kleemann, *Int. J. Mod. Phys. B* **7**, 2469 (1993).

⁴D. Viehland, J. F. Li, S. J. Jang, and L. E. Cross, *Phys. Rev. B* **43**, 8316 (1991).

⁵N. de Mathan, E. Husson, G. Calvarin, J. R. Gavarri, A. W. Hewat, and A. Morell, *J. Phys.: Condens. Matter* **3**, 8159 (1991).

⁶P. Bonneau, P. Garnier, E. Husson, and A. Morell, *Mater. Res. Bull.* **24**, 201 (1989).

⁷P. Bonneau, P. Garnier, G. Calvarin, E. Husson, J. R. Gavarri, A. W. Hewat, and A. Morell, *J. Solid State Chem.* **91**, 350 (1991).

⁸O. Noblanc, P. Gaucher, and G. Calvarin, *J. Appl. Phys.* **79**, 4291 (1996).

⁹B. Dkhil, J. M. Kiat, G. Calvarin, S. B. Vakhruhev, G. Balduinozzi, and E. Suart, *Phys. Rev. B* **65**, 024104 (2002).

¹⁰G. Calvarin, E. Husson, and Z. G. Ye, *Ferroelectrics* **165**, 349 (1995).

¹¹S. B. Vakhruhev, J. M. Kiat, and B. Dkhil, *Solid State Commun.* **103**(8), 477 (1997).

¹²K. Fujishiro, Y. Uesu, Y. Yamada, B. Dkhil, J. M. Kiat, and Y. Yamashita, *J. Korean Phys. Soc.* **32**, S964 (1998).

¹³J. Kreisel, B. Dkhil, P. Bouvier, and J. M. Kiat, *Phys. Rev. B* **65**, 172101 (2002).

¹⁴A. Lebon, H. Dammak, G. Calvarin, and I. Ould Ahmedou, *J.*

- Phys.: Condens. Matter **14**, 7035 (2002).
- ¹⁵N. Setter and L. E. Cross, J. Mater. Sci. **15**, 2478 (1980).
 - ¹⁶C. Malibert, B. Dkhil, J. M. Kiat, D. Durand, J. F. Bérar, and A. Spasojevic-de-Biré, J. Phys.: Condens. Matter **9**, 7485 (1997).
 - ¹⁷C. G. Stenger and F. Burggraaf, Phys. Status Solidi A **61**, 255 (1980).
 - ¹⁸L. Bellaiche, J. Padilla, and D. Vanderbilt, Phys. Rev. B **59**, 1834 (1999).
 - ¹⁹A. M. George, J. Iniguez, and L. Bellaiche, Nature (London) **413**, 54 (2001).
 - ²⁰L. Bellaiche, Curr. Opin. Solid State Mater. Sci. **6**, 19 (2002).
 - ²¹J. Iniguez and L. Bellaiche, Phys. Rev. Lett. **87**, 095503 (2001).
 - ²²B. Jaffe, W. R. Cook, and H. Jaffe, *Piezoelectric Ceramics* (Academic, London, 1971).
 - ²³J. Kuwata, K. Uchino, and S. Nomura, Jpn. J. Appl. Phys., Part 1 **21**, 1298 (1982).
 - ²⁴S. E. Park and T. R. Shrout, J. Appl. Phys. **82**, 1804 (1997).
 - ²⁵S. E. Park and T. R. Shrout, Jpn. J. Appl. Phys., Part 1 **36**, 1154 (1997).
 - ²⁶V. J. Tennery, K. W. Hang, and R. E. Novak, J. Am. Ceram. Soc. **51**, 671 (1968).
 - ²⁷Y. Yamashita, Jpn. J. Appl. Phys., Part 1 **33**, 5328 (1994).
 - ²⁸S. K. Mishra, D. Pandey, and A. P. Singh, Appl. Phys. Lett. **69**, 1707 (1996).
 - ²⁹V. A. Isupov, Solid State Commun. **17**, 1331 (1975).
 - ³⁰K. Kakegawa, J. Mohri, T. Takahashi, H. Yamamura, and S. Shirasaki, Solid State Commun. **24**, 769 (1977).
 - ³¹W. Cao and L. E. Cross, Phys. Rev. B **47**, 4825 (1993).
 - ³²B. Noheda, D. E. Cox, G. Shirane, J. A. Gonzalo, L. E. Cross, and S. E. Park, Appl. Phys. Lett. **74**, 2059 (1999).
 - ³³B. Noheda, D. E. Cox, G. Shirane, R. Guo, B. Jones, and L. E. Cross, Phys. Rev. B **61**, 8687 (2000).
 - ³⁴B. Noheda, Curr. Opin. Solid State Mater. Sci. **6**, 27 (2002).
 - ³⁵K. Fujishiro, R. Vlokh, Y. Uesu, Y. Yamada, J. M. Kiat, B. Dkhil, and Y. Yamashita, Jpn. J. Appl. Phys., Part 1 **37**(9B), 5246 (1998).
 - ³⁶D. Viehland, J. Appl. Phys. **88**, 4794 (2000).
 - ³⁷J. M. Kiat, Y. Uesu, B. Dkhil, M. Matsuda, C. Malibert, and G. Calvarin, Phys. Rev. B **65**, 064106 (2002).
 - ³⁸Y. Uesu, M. Matsuda, Y. Yamada, K. Fujishiro, D. E. Cox, B. Noheda, and G. Shirane, J. Phys. Soc. Jpn. **71**, 960 (2002).
 - ³⁹A. K. Singh and D. Pandey, J. Phys.: Condens. Matter **13**, L931 (2001).
 - ⁴⁰B. Noheda, D. E. Cox, G. Shirane, J. Gao, and Z. G. Ye, Phys. Rev. B **66**, 054104 (2002).
 - ⁴¹Z. G. Ye, B. Noheda, M. Dong, D. E. Cox, and G. Shirane, Phys. Rev. B **64**, 184114 (2001).
 - ⁴²D. La-Orautapong, B. Noheda, Z. G. Ye, P. M. Gehring, J. Toulouse, D. E. Cox, and G. Shirane, Phys. Rev. B **65**, 144101 (2002).
 - ⁴³L. Bellaiche, A. Garcia, and D. Vanderbilt, Phys. Rev. Lett. **84**, 5427 (2000).
 - ⁴⁴H. Fu and R. E. Cohen, Nature (London) **403**, 281 (2000).
 - ⁴⁵D. Viehland, J. Powers, L. E. Cross, and J. F. Li, Appl. Phys. Lett. **78**, 3508 (2001).
 - ⁴⁶D. Vanderbilt and M. H. Cohen, Phys. Rev. B **63**, 094108 (2001).
 - ⁴⁷Y. Yamashita, Jpn. J. Appl. Phys., Part 1 **32**, 5036 (1993).
 - ⁴⁸E. F. Alberta and A. S. Bhalla, Mater. Lett. **35**, 199 (1998).
 - ⁴⁹J. S. Kim, S. J. Kim, H. G. Kim, D. C. Lee, and K. Uchino, Jpn. J. Appl. Phys., Part 1 **38**, 1433 (1999).
 - ⁵⁰J. F. Bérar, G. Baldinozzi, CPD Newsletter **20**, 3 (1998).
 - ⁵¹A. Al-Barakaty and L. Bellaiche, Appl. Phys. Lett. **81**, 2442 (2002).
 - ⁵²R. Hemphill, L. Bellaiche, A. Garcia, and D. Vanderbilt, Appl. Phys. Lett. **77**, 3642 (2000).
 - ⁵³L. Bellaiche and D. Vanderbilt, Phys. Rev. B **61**, 7877 (2000).
 - ⁵⁴P. Hohenberg and W. Kohn, Phys. Rev. **136**, B864 (1964); W. Kohn and L. J. Sham, Phys. Rev. **140**, A1133 (1965).
 - ⁵⁵D. Vanderbilt, Phys. Rev. B **41**, 7892 (1990).
 - ⁵⁶L. Bellaiche, A. Garcia, and D. Vanderbilt, Ferroelectrics **266**, 41 (2002).
 - ⁵⁷K. Uchino, S. Nomura, L. E. Cross, S. J. Jang, and R. E. Newnham, J. Appl. Phys. **51**, 1142 (1980).
 - ⁵⁸J. M. Kiat, G. Baldinozzi, M. Dunlop, C. Malibert, B. Dkhil, C. Ménoret, O. Masson, and M. T. Fernandez-Diaz, J. Phys.: Condens. Matter **12**, 8411 (2000).
 - ⁵⁹R. J. Nemes, R. O. Piltz, W. F. Kuhs, Z. Tun, and R. Restori, Ferroelectrics **108**, 165 (1990).
 - ⁶⁰R. Blinc, J. Dolinsek, A. Gregorovic, B. Zalar, C. Filipic, Z. Kutnjak, A. Levstik, and R. Pirc, J. Phys. Chem. Solids **61**, 177 (2000).
 - ⁶¹V. Bobnar, Z. Kutnjak, R. Pirc, R. Blinc, and A. Levstik, Phys. Rev. Lett. **84**, 5892 (2000).
 - ⁶²I. Grinberg, V. R. Cooper, and A. M. Rappe, Nature (London) **419**, 909 (2002).
 - ⁶³W. Dmowski, M. K. Akbas, P. K. Davies, and T. Egami, J. Phys. Chem. Solids **61**, 229 (2000).
 - ⁶⁴D. L. Corker, A. M. Glazer, R. W. Whatmore, A. Stallard, and F. Fauth, J. Phys.: Condens. Matter **10**, 6251 (1998).
 - ⁶⁵B. Noheda, J. A. Gonzalo, L. E. Cross, R. Guo, S. E. Park, D. E. Cox, and G. Shirane, Phys. Rev. B **63**, 014103 (2000).
 - ⁶⁶D. Le Bellac, J. M. Kiat, and P. Garnier, J. Solid State Chem. **114**, 459 (1995).
 - ⁶⁷M. K. Durbin, E. W. Jacobs, and J. C. Hicks, Appl. Phys. Lett. **74**, 2848 (1999).
 - ⁶⁸V. Y. Topolov, Phys. Rev. B **65**, 094207 (2002).
 - ⁶⁹L. Mitoseriu, P. M. Vilarinho, and J. L. Baptista, Appl. Phys. Lett. **80**, 4422 (2002).